Inorganic Chemistry

Article

pubs.acs.org/IC

Surface Enhanced Raman Spectroelectrochemistry of a μ-Oxo Triruthenium Acetate Cluster: An Experimental and Theoretical Approach

Jonnatan J. Santos, Romulo A. Ando, Sergio H. Toma, Paola Corio, Koiti Araki, and Henrique E. Toma*

Instituto de Química, Universidade de São Paulo, Av. Prof. Lineu Prestes, 748, CEP 05508-000, São Paulo, São Paulo, Brazil

Supporting Information

ABSTRACT: Surface enhanced Raman spectroelectrochemistry (SERS) spectroelectrochemistry provides a very sensitive technique to investigate the vibrational characteristics of coordination compounds and their particular behavior under the influence of plasmonic surfaces, concomitant with the exploitation of their redox properties and electronic spectra. The results, however, depend upon the mechanisms involved in the intensification of Raman spectra associated with the electromagnetic, resonance Raman and charge-transfer excitation at the Fermi levels. By probing the model complex $[(Ru_3O)(CH_3COO)_6(4,4'\text{-bipy})_3]^n$ (n = 1, 0, −1) adsorbed onto rough gold electrode surfaces, contrasting SERS profiles were obtained at several successive redox potentials and oxidation states, which enables a critical discussion on the role of the complex interaction with the gold surface, and the influence of the specific electronic bands in the triruthenium acetate cluster. Density functional theory (DFT) and time-dependent DFT calculations were carried out for the complex bound to an Au_{20} cluster to show the participation of active lowest unoccupied molecular orbital levels centered on the gold atoms. The corresponding charge-transfer band was predicted around 1200 nm, which supports a charge-transfer interpretation for the SERS response observed at λ_{exc} = 1064 nm. The selective enhancement of the vibrational modes was discussed based on the Raman theoretical calculations.

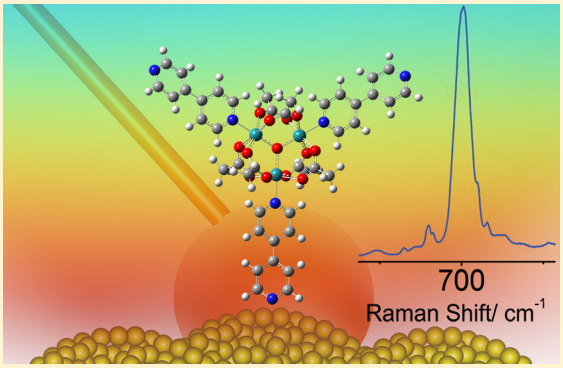

INTRODUCTION

Surface enhanced Raman spectroscopy (SERS) is opening exciting perspectives in inorganic chemistry by providing relevant information on metal complexes behavior under the influence of plasmonic surfaces such as in gold, silver, and copper nanostructures. As a matter of fact, the SERS effect can promote a huge enhancement of the Raman signals by up to 12 orders of magnitude to allow researchers to reach the single molecule detection limit in favorable cases. In association with electrochemistry, SERS can help increase understanding of the electronic and vibrational structures of complexes as a function of their oxidation states and improve the analysis of their interaction with the metal surfaces.

The nature of the SERS effect has been extensively investigated since the first observation by Fleischmann et al.[1] in 1974, of a huge enhancement of the Raman signals of adsorbed species, such as pyridine, on electrochemically roughened metal electrode surfaces. Such discovery was corroborated independently by Jeanmaire and Van Duyne,[2] and Albrecht and Creighton,[3] in 1977. Currently, the enhancement can be directly observed on metal nanoparticles. For this reason, SERS has become a subject of great interest in nanotechnology and allows important applications in materials and biological sciences. However, in spite of great progress, the nature of the SERS effect is not yet completely understood.

The discussion of SERS has been mostly concentrated on the electromagnetic mechanism (EM) associated with the molecular excitation at local fields of a metal surface. This mechanism seems to have a more general appeal because it is essentially governed by physical rules. The so-called charge-transfer or chemical mechanism (CT) has also been considered, but it is more complicated since it depends on the properties of the molecule and of the surface where it is adsorbed, as well as on the new kind of superficial complex generated between these species.[4−7] In addition, there is apparent confusion regarding the contribution of the resonance Raman (RR) mechanism to the SERS effect.

Recently, however, all the mechanisms have converged into a unified approach developed by Lombardi and Birke,[6] as expressed by the equation

$$R_{IFK}(\omega) = [\mu_{KI}\mu_{FK}h_{IF}\langle i|Q_k|f\rangle] / \{[(\varepsilon_1(\omega) + 2\varepsilon_m)^2 + \varepsilon_2^2](\omega_{FK}^2 - \omega^2 + \gamma_{FK}^2)(\omega_{IK}^2 - \omega^2 + \gamma_{IK}^2)\}$$

Received: August 3, 2015
Published: September 22, 2015

DOI: 10.1021/acs.inorgchem.5b01751
Inorg. Chem. 2015, 54, 9656−9663

In this unified theory, the surface-enhanced Raman intensity is expressed in terms of the square of the polarizability factor, $|R_{IFK}(\omega)|^2$, where I, F, and K refer, respectively, to the ground state, a charge-transfer state, and an excited molecular state of the molecule-metal system.[6,8] The denominator of the equation involves the product of three terms, each one representing a specific contribution to SERS. The first term, $[\varepsilon_1(\omega) - 2\varepsilon_m]^2 + \varepsilon_2^2$, involves the electromagnetic plasmon resonance at $\varepsilon_1(\omega) = -2\varepsilon_m$, corresponding to the EM mechanism. The second term, $(\omega_{FK}^2 - \omega^2 + \gamma_{FK}^2)$, involves the Fermi level dependent charge-transfer state (F) and promotes a charge-transfer resonance at $\omega = \omega_{FK}$, representing the CT mechanism. The third term, $(\omega_{IK}^2 - \omega^2 + \gamma_{IK}^2)$, involves the ground and excited states of the molecule and leads to the molecular resonance contribution at $\omega = \omega_{IK}$, corresponding to the RR mechanism. Therefore, the equation contemplates one, two, or three resonance mechanisms under the influence of the plasmon surface, which depends on the metal and adsorbed molecule characteristics, as well as on the excitation wavelengths, oscillator strengths, Fermi energies, and nanoparticles size.

In order to explore the unified theory in coordination chemistry, the choice of the transition metal complex is relevant for achieving a suitable combination of electrochemical, absorption, and Raman characteristics. The trinuclear μ-oxo ruthenium acetate cluster complexes, of general formula $[(Ru_3O)(CH_3COO)_6L_3]$, are particularly suitable. Structurally, they provide well-behaved examples of symmetric clusters that exhibit six acetate bridges and a central μ-oxo system connecting the three ruthenium ions, which leaves three axial interchangeable positions at the metal atoms.[9] By exploring the ligand substitution at the axial positions, one can build up a large number of structures, such as films,[10] dendrimers,[11,12] hybrid complexes,[13,14] modified quantum-dots,[15] or supramolecular species in association with different classes of molecules/complexes.[16]

Another important aspect of $[(Ru_3O)(CH_3COO)_6L_3]$ complexes is their very interesting electronic properties. The strong electronic delocalization of the complex (belonging to Robin-Day Class III type) yields four to five reversible one-electron redox processes between −2.0 to 2.0 V (vs SHE), modulated by the axial ligands (L).[17] The redox processes can be concomitantly probed by electronic UV−vis absorption and vibrational spectra, by means of spectroelectrochemical measurements. The redox state has a direct influence on the covalent bond between the ruthenium ions and the axial ligands. Ito, Abe, and Kubiak have extensively demonstrated how this influence is reflected in the infrared spectra of carbonyl complexes.[18,19] Sasaki et al. also elegantly explored the changes in the infrared behavior of self-assembled monolayers (SAM) on gold surfaces.[20,21]

In this work we selected the $[(Ru_3O)(CH_3COO)_6(4,4'\text{-bipy})_3]^n$ cluster species (Scheme 1), because it is well-characterized, and the ability of 4,4′-bipyridine ligand to bind to gold surface has already been explored in SERS studies with gold nanoparticles, focusing on the assembly of new hybrid supramolecular materials.[14] For new insight on the subject, our present focus centered on its SERS spectroelectrochemical behavior at textured electrode surfaces, as a function of the applied potentials and laser excitation wavelengths. In particular, considering the chemical, or charge-transfer effect, the dependence of the Raman spectrum with the metal Fermi level makes electrochemistry a better choice to investigate the behavior of the title complex, in the context of the SERS mechanisms involved. Additionally, we also performed detailed theoretical calculations to model and understand the nature of the species at the gold electrode surface. To the best of our knowledge, similar experimental and theoretical investigations involving transition metal complexes at the electrode level have never been reported before.

Scheme 1. Molecular Structure of the Complex $[(Ru_3O)(CH_3COO)_6(4,4'\text{-bipy})_3]$ (Left) and Structure Optimized by Density Functional Theory Calculation (Right)

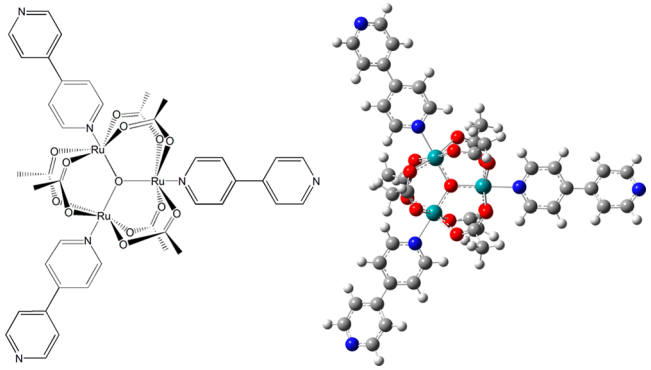

EXPERIMENTAL SECTION

Materials. Deionized water with resistivity of 18 MΩ was obtained from a Milli-Q purification system. Acetonitrile (ACN), tetrabutylammonium hexafluorophosphate ($TBAPF_6$, 98%), and potassium chloride (KCl, 99%) were obtained from Sigma-Aldrich.

Measurements. Electrochemical measurements were performed with an Auto-Lab PGSTAT30 (EcoChemie, Netherlands) potentiostat/galvanostat. Cyclic voltammetry (CV) and differential pulse voltammetry (DPV) experiments were carried out in acetonitrile solution using a conventional three-electrodes configuration, consisting of an Ag/Ag^+ (0.01 mol L^{-1} $AgNO_3$) reference electrode (E^o = 0.553 V vs SHE, Fc/Fc^+ = 0.07 V vs Ag/Ag^+), a coiled platinum wire auxiliary electrode and 0.2 cm^2 platinum working electrode and $TBAPF_6$ (0.1 mol L^{-1}) as supporting electrolyte. All the reported potentials were converted into the SHE scale. The measurements of the Vis-NIR spectra, which compose the spectroelectrochemical information, were performed with an electrochemical cell with quartz window. The reflectance spectra were recorded with a FieldSpec3 (Analytical Spectral Devices, USA) spectroradiometer.

Raman spectroelectrochemistry was performed in a cell made of Teflon, equipped with a gold working electrode, a platinum wire as auxiliary electrode, and a conventional Luggin capillary arrangement with an Ag/AgCl wire as reference system which contained KCl 3.5 mol L^{-1}. The Raman spectra were acquired using two different apparati: a Raman spectrometer microscope from Renishaw model inVia equipped with a 63× water immersion objective (NA = 0.9) and two different laser lines for excitation, 633 nm (a He−Ne source (Renishaw RL6333)) and a 785 nm (solid state laser), and a Raman spectrophotometer from Jobin-Yvon model T64000 equipped with a 50× objective (NA = 0.45) and a solid state laser with 1064 nm line. The fixed electrochemical measurements were accomplished with an EG&G potentiostat model PAR-273.

Procedures. The $[(Ru_3O)(CH_3COO)_6(4,4'\text{-bipy})_3]PF_6$ complex was synthesized as previously published.[14,22] Electrochemical activation of gold electrode was carried out by sweeping 25 oxidation/reduction cycles in 0.1 mol L^{-1} KCl in the potential range from −0.3 to +1.3 V vs Ag/AgCl at a scan rate of 0.1 V s^{-1}. The rough gold electrode was modified by application of a drop of the $[(Ru_3O)(CH_3COO)_6(4,4'\text{-bipy})_3]PF_6$ solution (1.0×10^{-6} mol L^{-1}) for at least 15 min and was then washed with water and used for the Raman spectroscopy measurements. The specific redox states of the complex were generated by applying a suitable potential for 30s.

DOI: 10.1021/acs.inorgchem.5b01751
Inorg. Chem. 2015, 54, 9656−9663

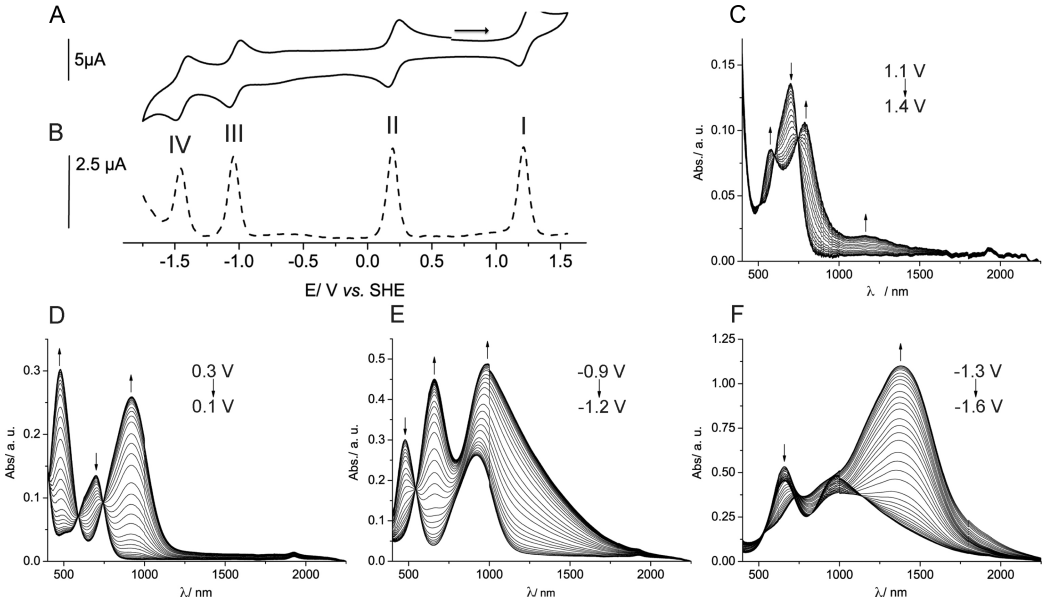

Figure 1. Electrochemistry and electronic spectroelectrochemistry of $[(Ru_3O)(CH_3COO)_6(4,4'\text{-bipy})_3]PF_6$. (A) CV of 1.0×10^{-3} mol L^{-1} of the complex in 0.1 mol L^{-1} $TBAPF_6$ and acetonitrile; scan rate 0.05 V s^{-1} and (B) 0.02 V s^{-1} for DPV; (C) electronic spectra for process $Ru_3^{III,III,III} \rightarrow Ru_3^{III,III,IV}$; (D) $Ru_3^{III,III,III} \rightarrow Ru_3^{II,III,III}$; (E) $Ru_3^{II,III,III} \rightarrow Ru_3^{II,II,III}$; and (F) $Ru_3(4,4'\text{-bipy} \rightarrow 4,4'\text{-bipy}^{\bullet-})$.

Theoretical Calculation. DFT calculations were performed using Gaussian 03 (Gaussian Inc., Wallingford, CT, USA) software. The ground state geometries were fully optimized by DFT with the B3LYP hybrid functional (Becke's gradient corrected exchange correlation in conjunction with the Lee–Yang–Parr correlation functional with three parameters).[23] The calculations of the ruthenium complex and of its gold (Au_{20}) adduct were performed using the gen keyword, where the atoms (C, H, N, and O) were calculated with the 6-311++G(d,p) basis set and the ruthenium and gold atom with the LANL2DZ basis set considering a pseudo potential. The vibrational frequency analyses were carried out, and no imaginary frequencies were found, which indicated that the optimized geometries were in a minimum on the potential energy surface. The simulated Raman spectra were plotted with a bandwidth of 5 cm^{-1} and a scaling factor of 0.9679 for the calculated harmonic vibrational wavenumbers from the functional (B3LYP) and the 6-311++G(d,p) basis set. The vertical excitation energies were determined by time-dependent density functional theory (TD-DFT) implemented in Gaussian 03.

RESULTS AND DISCUSSION

Electrochemistry and Vis-NIR Spectroelectrochemistry. A classical description of the molecular orbitals for the $[(Ru_3O)(CH_3COO)_6(py)_3]^+$ complex has been reported by Cotton and Norman,[24] who considered a model essentially centered on the triangular Ru_3O chromophore. For the formal oxidation state $Ru_3^{III,III,III}$, the following sequence of orbital symmetry representations has been proposed: $(a_2'')^2(e')^4(a_1')^2(e')^4(e'')^4(a_2')$. In addition, there is an empty low-lying a_2'' orbital, which participates in the electronic transitions in this complex.

The electronic Vis-UV spectroelectrochemistry of analogous compounds has already been reported.[25,26] However, for the purposes of this work, the electrochemical and electronic spectroelectrochemical behavior of the $[(Ru_3O)(CH_3COO)_6(4,4'\text{-bipy})_3]PF_6$ complex was reinvestigated in order to expand the spectral range to include the near-infrared (NIR), as shown in Figure 1.

In the cyclic voltammograms (Figure 1A), four reversible one-electron electrochemical processes are corroborated by the similar peak heights and bandwidths of the differential pulse voltammograms in Figure 1B.

Redox process I, shown in Figure 1, corresponds to the $Ru_3^{III,III,III} \rightarrow Ru_3^{III,III,IV}$ step, at $E_{1/2}$ = 1.21 V vs SHE. The electronic spectral response (Figure 1C) for this oxidation process results in the decay of the intracluster band around 698 nm and the increase of two bands, at 580 and 785 nm (Figure 1C). This change reflects the removal of one unpaired electron in the HOMO (a_2') orbital in the complex in the oxidation process. The abstraction of this electron turns the a_2' orbital into a new LUMO and allows a new low energy intracluster transition (785 nm), while the remaining occupied orbitals are stabilized, which increases the energy of the second intracluster band.

Process II in Figure 1D corresponds to the $Ru_3^{III,III,III} \rightarrow Ru_3^{II,III,III}$ redox step at $E_{1/2}$ = 0.20 V vs SHE and involves the insertion of one electron into the a_2' orbital, which now becomes filled with two electrons. As a consequence, the corresponding band at 698 nm disappears. The reorganization of the energy levels leads to two new bands at 483 and 923 nm.

Process III in Figure 1D is assigned to the $Ru_3^{II,III,III} \rightarrow Ru_3^{II,II,III}$ redox process at $E_{1/2}$ = −1.04 V vs SHE. It leads to a red shift of the band at 923 to 980 nm and to the appearance of a new band at 660 nm; this new species, analogous to $Ru_3^{III,III,III}$, is paramagnetic.

It should be noted that the redox potentials which correspond to steps I, II, and III are separated by 1.01 and 1.24 V, respectively, and reflect a dramatic role of the electronic delocalization in the triangular cluster moiety, as expected for a typical Robin-Day class III mixed valence system. In contrast, the electrochemical process which corresponds to process IV (Figure 1F) departs from the previous trends and exhibits a potential difference of 0.41 V. This process can be assigned to the 4,4′-bipy → 4,4′-bipy$^{\bullet-}$ reduction wave at $E_{1/2}$ = −1.45 V vs SHE. The reduction of the 4,4′-bipyridine ligand forms an anion radical coordinated to a highly conjugated system and so generates a broad, low energy band in the NIR region. Although in the cyclic voltammogram the observed wave

DOI: 10.1021/acs.inorgchem.5b01751
Inorg. Chem. 2015, 54, 9656−9663

corresponds to the reduction of a single 4,4′-bipy ligand, in the spectroelectrochemical measurements more than one ligand can be involved, because of the long time scale of the experiments.

Although the electrochemical processes in this complex seem rather simple, which four successive, reversible one-electron steps the electronic spectra are actually very complicated since there are distinct energy levels localized on the central cluster moiety, the peripheral 4,4′-bipyridine ligands,[26,27] and the gold atoms.

Raman Spectroelectrochemistry. The Raman measurements were carried out on a gold disk electrode previously activated by oxidation/reduction cycles (Figure 2A) in order to increase the surface roughness and to generate a nanostructured surface capable of serving as a SERS-active substrate. The surface activation leads to a new band around 520 nm, very similar to the plasmon resonance bands observed for gold nanoparticles in solution.[14] The corresponding spectrum recorded after adsorption of the ruthenium cluster complex is shown in Figure 2B. As can be seen in the figure, the molecular contribution to the electronic spectrum is not apparent because the complex is only present at the electrode surface, and its optical absorptivity is much smaller in comparison with the extinction coefficients of the plasmonic rough surface.

In contrast with the electronic spectra, the presence of the adsorbed complex at the gold surface can be readily detected by the SERS effect, as shown in Figure 3. Very strong signals appear in the Raman spectra after adsorption of the complex on the electrochemically conditioned electrode.

After activation, the SERS effect of the nanostructured electrode surface modified with the complex was monitored by changing the applied potentials in order to convert the species into different redox states. The SERS spectra were recorded at several excitation wavelengths.

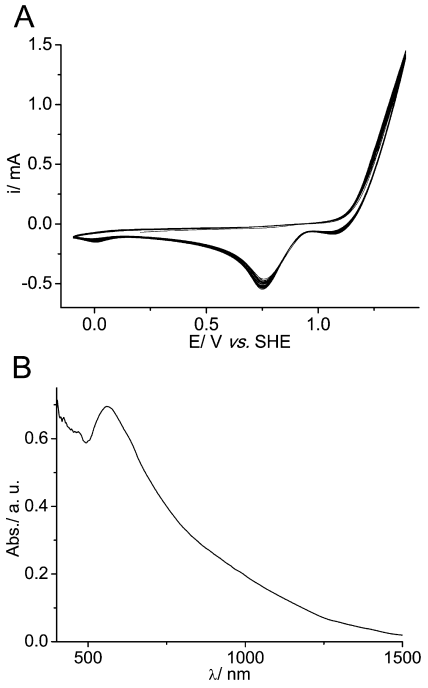

Figure 2. (A) Electrochemical conditioning of the flat gold electrode ([KCl] = 0.1 mol L^{-1} and v = 0.10 V s^{-1}) and (B) its electronic reflectance spectrum after the conditioning in the presence of the cluster species, showing the plasmon resonance peak at 520 nm and a weak shoulder around 1000 nm.

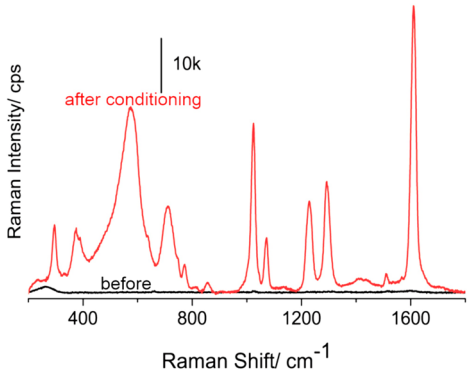

Figure 3. SERS response of the electrochemically conditioned gold electrode before (black) and after (red) adsorbing the ruthenium cluster complex (λ_{exc} = 785 nm).

In order to facilitate the discussion, the measured SERS spectra are displayed together with the corresponding electronic spectra of the complex obtained in solution. The SERS spectra obtained with three different laser sources for excitation are shown in Figures 4, 5, and 6.

The Raman/SERS spectra of the $[(Ru_3O)(CH_3COO)_6(4,4'\text{-bipy})_3]^+$ species, or $Ru_3^{III,III,III}$, (Figure 4) exhibit the characteristic vibrational bands of the 4,4′-bipyridine ligand[28,29] at 1613

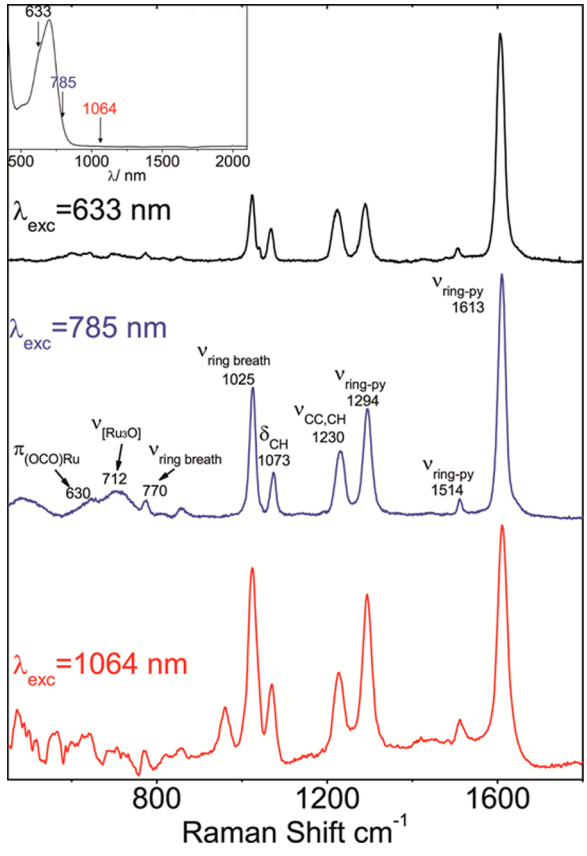

Figure 4. Raman spectroelectrochemistry of $[(Ru_3O)(CH_3COO)_6(4,4'\text{-bipy})_3]^+$ obtained by application of 0.40 V (vs SHE) on the electrode with three different lasers λ_{exc} = 633 nm (black); λ_{exc} = 785 nm (blue); and λ_{exc} = 1064 nm (red). The electronic spectrum of the complex in solution is shown in the inset.

DOI: 10.1021/acs.inorgchem.5b01751
Inorg. Chem. 2015, 54, 9656−9663

and 1512 ($\nu_{ring,py}$), 1294 (ν_{ring}, δCH), 1230 (νC−C, δCH_{py}, $\nu_{ring,py}$), 1073 (δCH, ν_{ring}), 1025 and 770 ($\nu_{ring\ breathing}$), and of the ruthenium acetate moiety, at 712 (δ_sOCO, Ru_3O) and 643 cm^{-1} (πOCO, Ru_3O). The excitation wavelengths at 633 and 785 nm are close to the gold surface plasmon band shown in Figure 2A and are also in resonance with the intracluster band at 690 nm, thus fulfilling the resonance conditions for the EM-SERS and RR-SERS mechanisms. Surprisingly, however, SERS bands can also be observed at λ_{exc} 1064 nm, which is far from the surface plasmon band (Figure 2B), and there is no absorption band for the $Ru_3^{III,III,III}$ complex. However, there is a coincidence with the shoulder in the extinction profile for the rough gold electrode, which suggests that this new feature can play a significant role in the SERS effect.

The SERS spectra of the complex monitored at 0.10 V (vs. SHE) corresponds to the $Ru_3^{II,III,III}$ oxidation state and exhibits the characteristic vibrational bands of the 4,4′-bipyridine ligand and of the ruthenium acetate moiety, although just slightly shifted in relation to the adsorbed $Ru_3^{III,III,III}$ species, as shown in Figure 5. However, the changes in the SERS profiles in this

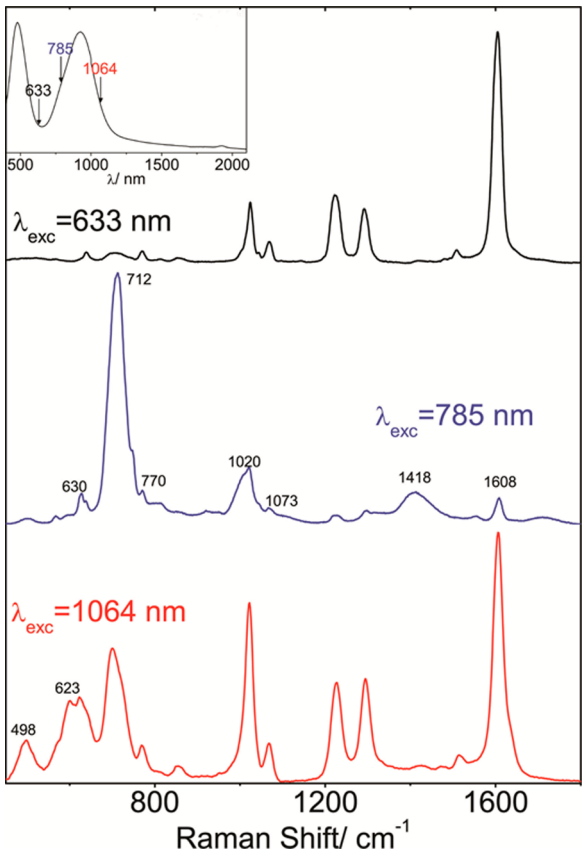

Figure 5. Raman spectroelectrochemistry of $[(Ru_3O)(CH_3COO)_6(4,4'\text{-bipy})_3]^0$ obtained by application of 0.10 V (vs SHE) on the electrode with three different lasers λ_{exc} = 633 nm (black); λ_{exc} = 785 nm (blue); and λ_{exc} = 1064 nm (red). The electronic spectrum of the complex in solution is shown in the inset.

case are quite remarkable. The SERS spectrum recorded at λ_{exc} = 633 nm seems quite similar to those observed for $Ru_3^{III,III,III}$ species. A close inspection of the electronic spectrum shown in Figure 5 reveals that at this particular wavelength there is only a poor overlap with the laser wavelength close to the minimum of the absorption band at 500 nm. Presumably, the electromagnetic mechanism predominates at this wavelength. However, at λ_{exc} = 785 nm the observed SERS profile is completely distinct and exhibits a huge enhancement of the vibrational peak at 712 cm^{-1} due to $\delta_s(Ru_3O)$, which reflects the resonance with the intracluster band at 900 nm. On the other hand, at λ_{exc} = 1064 nm, the SERS profile exhibits a new distinct profile which resembles a mixture of the 633 and 785 nm excitation profiles, but with an additional enhancement of the $\delta(Ru_3O)$ and ν(Ru−OCO) peaks at 623 and 497 cm^{-1}. This result indicates the contribution of a new resonance in the near-infrared region.

Finally, the SERS spectra (Figure 6) monitored at −1.20 V are assigned to the $Ru_3^{II,II,III}$ cluster complex and exhibit the

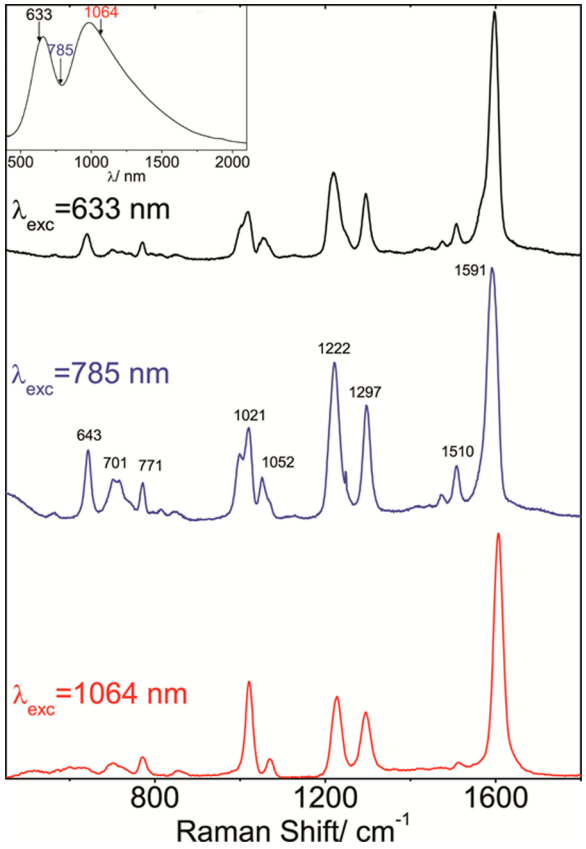

Figure 6. Raman spectroelectrochemistry of $[(Ru_3O)(CH_3COO)_6(4,4'\text{-bipy})_3]^-$ obtained by application of −1.20 V (vs SHE) on the electrode with three different lasers λ_{exc} = 633 nm (black); λ_{exc} = 785 nm (blue); and λ_{exc} = 1064 nm (red). The electronic spectrum of the complex in solution is shown in the inset.

same SERS profile at λ_{exc} 633 nm as observed for the $Ru_3^{III,III,III}$ and $Ru_3^{II,III,III}$ species in Figures 4 and 5, which supports a possible EM mechanism (Figure 6). On the other hand at 785 nm, the wavelength is centered exactly in the valley formed by the superimposition of the complex two absorption bands, which indicates the possibility of the influence of both transitions in the SERS spectra, via the RR mechanism. Surprisingly, the SERS profile at 1064 nm is similar to that observed at 633 nm, which indicates the predominance of the EM mechanism.

It should be noted that the peak at 711 cm^{-1} is related to the $[Ru_3O]$ center, as previously reported by Cannon.[30] Toma[26] has published a preresonant Raman spectrum of a similar complex substituted with pyrazine, and Kubiak characterized the dimers of triruthenium clusters[31,32] by electronic

DOI: 10.1021/acs.inorgchem.5b01751
Inorg. Chem. 2015, 54, 9656−9663

spectroelectrochemistry and resonance Raman. In all these cases, the studies were performed by normal resonance Raman spectroscopy, without surface enhancement effect. The SERS spectra in current work indicate a very strong enhancement of the 711 cm^{-1} peak, for the $Ru_3^{II,III,III}$ species, at λ_{exc} = 785 nm, an observation that has never been reported before.

In summary, the excitations at 633 nm for the complexes in the $Ru_3^{III,III,III}$, $Ru_3^{II,III,III}$, and $Ru_3^{II,II,III}$ oxidation states exhibit similar SERS profiles and support a dominant EM mechanism at this wavelength, corroborated by the proximity to the surface plasmon band (Figure 2B). At λ_{exc} = 785 nm, the SERS profiles obtained as a function of the oxidation state are differentiated and indicate the predominant contribution of the resonances with the existing absorption bands, thus supporting the RR mechanism. The SERS profiles obtained by the excitation at 1064 nm depart from these two hypotheses and suggest the existence of a new resonance promoted by a possible charge-transfer mechanism, which involves the interaction of the ruthenium cluster and the gold plasmon levels at the interface. In order to elucidate this point, we carried out a detailed molecular orbital calculation for a model ruthenium cluster and gold surface complex. An assembly of 20 gold atoms was employed to simulate the orbitals at the gold surface.

Theoretical Calculations. Molecular orbital calculations for isolated triruthenium cluster complexes have already been reported by Kubiak et al.,[33] Toma et al.[34] and recently by Uosaki et al.[35] Here, in order to investigate the influence of the gold surface in the Raman spectrum, we performed DFT and TD-DFT calculations for the $[(Ru_3O)(CH_3COO)_6(4,4'bipy)_3]$ cluster at the $Ru_3^{II,III,III}$ formal oxidation state, bound to a gold cluster species encompassing 20 atoms. Such an approach is relevant, since gold and silver clusters[36,37] have been frequently involved in the discussion of the chemical (CT) mechanism of SERS. The results can be seen in Table 1 and Table 2.

Table 1. Composition of the Frontier Orbitals of the Isolated Complex $[(Ru_3O)(CH_3COO)_6(4,4'\text{-bpy})_3]$

			composition/%			
orbital number	MO	MO, E (eV)	μ-O	Ru	Ac	4,4′-bpy
251	L+6	−0.023	0	1	0	99
250	L+5	−0.023	0	0	1	99
249	L+4	−0.024	0	0	1	99
248	L+3	−0.062	4	12	0	84
247	L+2	−0.066	0	3	0	97
246	L+1	−0.067	0	3	0	97
245	LUMO	−0.102	20	57	3	20
244	HOMO	−0.170	0	77	23	0
243	H-1	−0.170	0	78	22	0
242	H-2	−0.179	0	89	11	0
241	H-3	−0.185	0	82	11	7
240	H-4	−0.185	0	83	11	6
239	H-5	−0.189	5	84	8	3
238	H-6	−0.190	5	84	8	3

The calculations shown in Table 1 for the isolated complex indicate that the Mülliken population in the HOMO levels is essentially centered on the ruthenium atoms (77%) and partly on the acetate ligands (23%). On the other hand, the LUMO orbital (MO 245) is composed by ruthenium atoms (57%) and incorporates a significant contribution from the 4,4′-bipyridine (20%) and the oxo-bridge (20%) ligands. The strong band at 900 nm corresponds to the 241 → 245 transition.

Table 2. Composition of the Frontier Orbitals of the Complex $[(Ru_3O)(CH_3COO)_6(4,4'\text{-bpy})_3]$ Bound to an Au_{20} Cluster

				composition/%			
orbital number	MO	MO, E (eV)	μ-O	Ru	Ac	4,4′-bpy	Au
441	L+6	−0.103	0	0	0	2	98
440	L+5	−0.106	0	0	0	0	100
439	L+4	−0.106	0	0	0	0	100
438	L+3	−0.114	17	47	3	23	10
437	L+2	−0.116	1	2	0	1	96
436	L+1	−0.116	1	3	0	2	94
435	LUMO	−0.118	0	0	0	1	99
434	HOMO	−0.176	0	76	24	0	0
433	H-1	−0.176	0	76	24	0	0
432	H-2	−0.187	0	87	13	0	0
431	H-3	−0.190	0	83	12	5	0
430	H-4	−0.191	0	82	12	6	0
429	H-5	−0.196	5	84	7	4	0
428	H-6	−0.196	5	84	7	4	0

On the other hand, the calculations performed with the complex bound to the gold atoms indicate that the LUMO Mülliken populations exhibit a large electronic displacement from the bridging 4,4′-bipyridine ligand to the gold atoms, as compared to the free complex (Figure 7, MO 438). In addition, MO 436 exhibits the Mülliken population entirely centered on the gold atoms. These results clearly indicate a strong interaction between the ruthenium cluster and the gold surface, and provide a strong argument which favors the occurrence of the *chemical or charge-transfer effect* at the interface.

While the 430 → 438 and 431 → 438 transitions are typical of the intracluster transitions observed for the isolated complexes, the TD-DFT calculations for the complex bound to the gold cluster reveal a nonconventional charge-transfer transition from MO 428 (cluster centered) to MO 436 (gold centered) at 1207 nm. This transition can explain the spectral features observed in Figure 7 and allows understanding of the SERS profiles recorded at λ_{exc} = 1064 nm.

The theoretical Raman spectrum of the $[(Ru_3O)(CH_3COO)_6(4,4'\text{-bipy})_3]\text{-}Au_{20}$ complex has also been obtained as shown in Figure 8. It exhibits a strong correlation with the experimental spectrum.

As shown in Figure 9, the normal mode calculations demonstrate that the most strongly enhanced bands, e.g., at 1651, 1337, and 1270 cm^{-1}, are associated with the bipyridine ligands directly bound to the gold surface. As a matter of fact, the ν(C−C) band located at 1651 cm^{-1} has been predicted[29] to be the most intense one in previous SERS studies due the close proximity to the gold surface. On the other hand, the modes at 1270 and 1337 cm^{-1} can be used to probe the complex binding orientation at the gold surface. While the 1337 cm^{-1} band involves a vibrational mode localized on a single 4,4′-bipy moiety, the peak at 1270 cm^{-1} involves a similar vibrational mode which encompasses the two 4,4′-bipy ligands in the complex (see Figure 9). The vibrational band at 1337 cm^{-1} is more intense, as expected for the binding of just one ligand to the gold surface. However, after the reduction of the metal complex, the affinity of neutral complex to the surface should increase and facilitates the binding of a second 4,4′-bipy ligand, which leads to the enhancement of the 1270 cm^{-1} band. Conversely, the second reduction process should also increase

DOI: 10.1021/acs.inorgchem.5b01751
Inorg. Chem. 2015, 54, 9656−9663

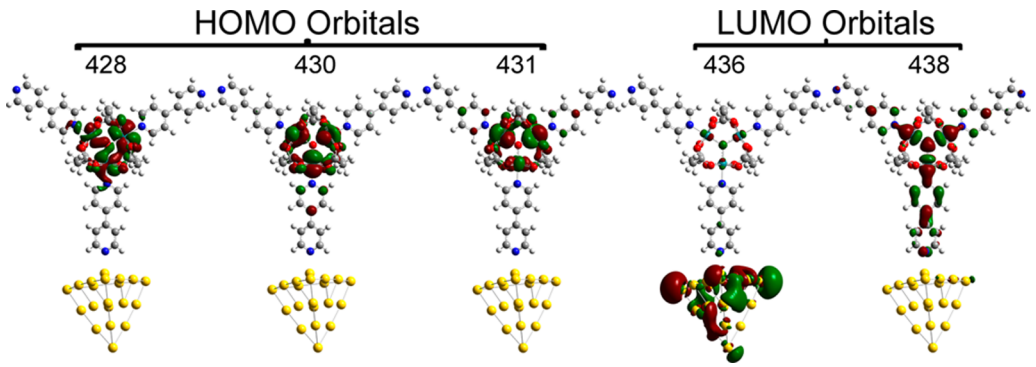

Figure 7. Contour plots of MOs involved in the electronic transitions obtained by TD-DFT calculations.

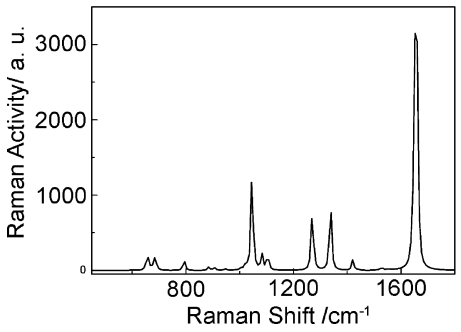

Figure 8. Simulated Raman spectrum of $[(Ru_3O)(CH_3COO)_3(4,4'\text{-bipy})_3]\text{-}Au_{20}$ complex.

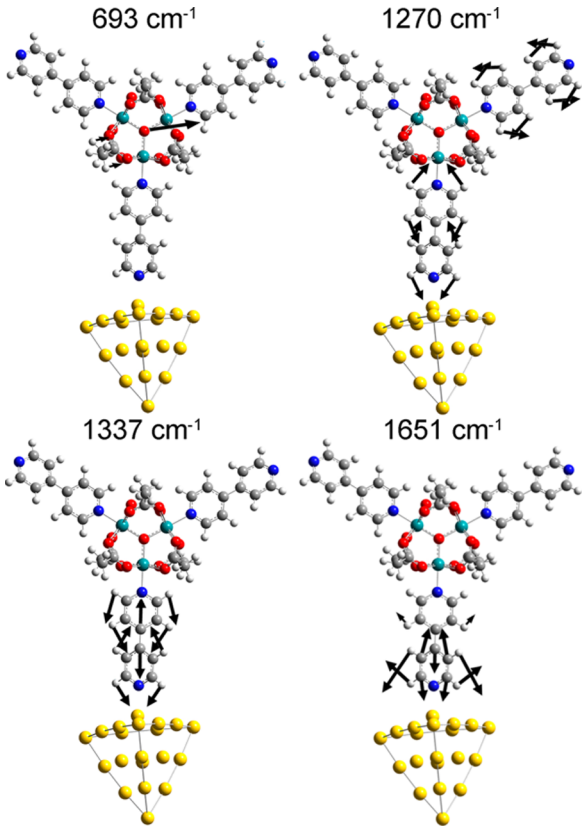

Figure 9. Main vibrational modes of $[(Ru_3O)(CH_3COO)_3(4,4'\text{-bipy})_3]\text{-}Au_{20}$ complex.

the soft character of the 4,4′-bipy ligand and enhance further the intensity of this band.

CONCLUSION

SERS spectroelectrochemical profiles can be conveniently exploited by adsorbing the chromophore species onto a rough texture, which are apparently nanostructures previously formed at conditioned gold electrodes. The advantage of this approach is the possibility of detection of the SERS signals directly at the electrodes in conjunction with the applied potentials in order to generate and to probe the adsorbed molecules specific redox states.

The comparison of the SERS signals obtained in several redox states, and at several excitation wavelengths, allows the evaluation and discrimination of the occurrence of the electromagnetic, resonance Raman and charge-transfer mechanisms at the electrode surface.

TD-DFT calculations were able to reproduce the SERS spectra, allowing the detection of a LUMO level localized on the Au_{20} gold cluster, and corroborate the occurrence of a chemical, or charge-transfer mechanism, particularly for the excitation at 1064 nm.

The most strongly enhanced vibrational modes are associated with the ligands directly bound to the gold surface, and their SERS profiles can be used to probe their specific binding modes.

ASSOCIATED CONTENT

Supporting Information

The Supporting Information is available free of charge on the ACS Publications website at DOI: 10.1021/acs.inorgchem.5b01751.

Figure S1. ^{1}H NMR spectrum of $[Ru_3O(CH_3COO)_6(4,4'\text{-bpy})_3]PF_6$ in deuterated acetone. Figure S2. ESI-MS spectrum of $[Ru_3O(CH_3COO)_6(4,4'\text{-bpy})_3]PF_6$. Figure S3. Contour plots of MOs of $[Ru_3O(CH_3COO)_6(4,4'\text{-bpy})_3]$. Figure S4. Contour plots of MOs of Au_{20}-$[Ru_3O(CH_3COO)_6(4,4'\text{-bpy})_3]$. Table S1. Assignments for Raman bands for the complex with different charges using laser excitation at λ_{exc} = 633 nm. Table S2. ibidem, at λ_{exc} = 785 nm. Table S3. ibidem, at λ_{exc} = 1064 nm. Table S4. Assignments for Raman bands for the complex $[Ru_3O(CH_3COO)_6(4,4'\text{-bpy})_3]\text{-}Au_{20}$ calculated by DFT (PDF)

AUTHOR INFORMATION

Corresponding Author

*E-mail: henetoma@iq.usp.br.

Notes

The authors declare no competing financial interest.

DOI: 10.1021/acs.inorgchem.5b01751
Inorg. Chem. 2015, 54, 9656−9663

■ ACKNOWLEDGMENTS

The authors thank the financial support from FAPESP and CNPq.

■ REFERENCES

(1) Fleischmann, M.; Hendra, P. J.; McQuillan, A. J. *Chem. Phys. Lett.* **1974**, *26*, 163−166.
(2) Jeanmaire, D. L.; Vanduyne, R. P. *J. Electroanal. Chem. Interfacial Electrochem.* **1977**, *84*, 1−20.
(3) Albrecht, M. G.; Creighton, J. A. *J. Am. Chem. Soc.* **1977**, *99*, 5215−5217.
(4) Rubim, J. C.; Corio, P.; Ribeiro, M. C. C.; Matz, M. *J. Phys. Chem.* **1995**, *99*, 15765−15774.
(5) Rubim, J. C.; Temperini, M. L. A.; Corio, P.; Sala, O.; Jubert, A. H.; Chacon-Villalba, M. E.; Aymonino, P. J. *J. Phys. Chem.* **1995**, *99*, 345−355.
(6) Lombardi, J. R.; Birke, R. L. *Acc. Chem. Res.* **2009**, *42*, 734−742.
(7) Corio, P.; Andrade, G. F. S.; Diogenes, I. C. N.; Moreira, I. S.; Nart, F. C.; Temperini, M. L. A. *J. Electroanal. Chem.* **2002**, *520*, 40−46.
(8) Lombardi, J. R.; Birke, R. L. *J. Chem. Phys.* **2012**, *136*, 144704.
(9) Toma, H. E.; Araki, K.; Alexiou, A. D. P.; Nikolaou, S.; Dovidauskas, S. *Coord. Chem. Rev.* **2001**, *219*, 187−234.
(10) Toma, S. H.; Santos, J. J.; Velho, R. G.; Nakamura, M.; Toma, H. E.; Araki, K. *Electrochim. Acta* **2012**, *66*, 287−294.
(11) Toma, S. H.; Santos, J. J.; Nikolaou, S.; Araki, K.; Toma, H. E. *Inorg. Chim. Acta* **2012**, *390*, 148−153.
(12) Nikolaou, S.; Toma, H. E. *Eur. J. Inorg. Chem.* **2008**, *2008*, 2266−2271.
(13) Canzi, G.; Kubiak, C. P. *J. Phys. Chem. C* **2012**, *116*, 6560−6566.
(14) Toma, S. H.; Santos, J. J.; Araki, K.; Toma, H. E. *Eur. J. Inorg. Chem.* **2011**, *2011*, 1640−1648.
(15) Morris-Cohen, A. J.; Aruda, K. O.; Rasmussen, A. M.; Canzi, G.; Seideman, T.; Kubiak, C. P.; Weiss, E. A. *Phys. Chem. Chem. Phys.* **2012**, *14*, 13794−13801.
(16) Toma, H. E.; Araki, K. *Prog. Inorg. Chem.* **2009**, *56*, 379−485.
(17) Alexiou, A. D. P.; Toma, H. E. *J. Chem. Res. Synop.* **1993**, 464−465.
(18) Ito, T.; Hamaguchi, T.; Nagino, H.; Yamaguchi, T.; Washington, J.; Kubiak, C. P. *Science* **1997**, *277*, 660−663.
(19) Ito, T.; Hamaguchi, T.; Nagino, H.; Yamaguchi, T.; Kido, H.; Zavarine, I. S.; Richmond, T.; Washington, J.; Kubiak, C. P. *J. Am. Chem. Soc.* **1999**, *121*, 4625−4632.
(20) Abe, M.; Michi, T.; Sato, A.; Kondo, T.; Zhou, W.; Ye, S.; Uosaki, K.; Sasaki, Y. *Angew. Chem., Int. Ed.* **2003**, *42*, 2912−2915.
(21) Ye, S.; Zhou, W.; Abe, M.; Nishida, T.; Cui, L.; Uosaki, K.; Osawa, M.; Sasaki, Y. *J. Am. Chem. Soc.* **2004**, *126*, 7434−7435.
(22) Toma, H. E.; Alexiou, A. D. P.; Nikolaou, S.; Dovidauskas, S. *Magn. Reson. Chem.* **1999**, *37*, 322−324.
(23) Lee, C. T.; Yang, W. T.; Parr, R. G. *Phys. Rev. B: Condens. Matter Mater. Phys.* **1988**, *37*, 785−789.
(24) Cotton, F. A.; Norman, J. G.; Spencer, A.; Wilkinson, G. *J. Chem. Soc. D* **1971**, 967.
(25) Toma, H. E.; Cipriano, C. *J. Electroanal. Chem. Interfacial Electrochem.* **1989**, *263*, 313−322.
(26) Toma, H. E.; Cipriano, C. *Monatsh. Chem.* **1989**, *120*, 815−820.
(27) Baumann, J. A.; Salmon, D. J.; Wilson, S. T.; Meyer, T. J.; Hatfield, W. E. *Inorg. Chem.* **1978**, *17*, 3342−3350.
(28) Wandlowski, T.; Ataka, K.; Mayer, D. *Langmuir* **2002**, *18*, 4331−4341.
(29) Zhuang, Z.; Cheng, J.; Wang, X.; Zhao, B.; Han, X.; Luo, Y. *Spectrochim. Acta, Part A* **2007**, *67*, 509−516.
(30) Johnson, M. K.; Powell, D. B.; Cannon, R. D. *Spectrochim. Acta. A* **1981**, *37*, 995−1006.
(31) Rocha, R. C.; Brown, M. G.; Londergan, C. H.; Salsman, J. C.; Kubiak, C. P.; Shreve, A. P. *J. Phys. Chem. A* **2005**, *109*, 9006−9012.
(32) Londergan, C. H.; Rocha, R. C.; Brown, M. G.; Shreve, A. P.; Kubiak, C. P. *J. Am. Chem. Soc.* **2003**, *125*, 13912−13913.
(33) Londergan, C. H.; Kubiak, C. P. *J. Phys. Chem. A* **2003**, *107*, 9301−9311.
(34) Toma, H. E.; Alexiou, A. D. P.; Dovidauskas, S. *Eur. J. Inorg. Chem.* **2002**, *2002*, 3010−3017.
(35) Zhang, H. X.; Sasaki, Y.; Zhang, Y.; Ye, S.; Osawa, M.; Abe, M.; Uosaki, K. *Inorg. Chem.* **2014**, *53*, 1288−1294.
(36) Zhang, X.; Wang, P.; Sheng, S.; Zhang, L.; Fang, Y. *Spectrochim. Acta, Part A* **2014**, *121*, 430−435.
(37) Zhao, L.; Jensen, L.; Schatz, G. C. *J. Am. Chem. Soc.* **2006**, *128*, 2911−2919.

DOI: 10.1021/acs.inorgchem.5b01751
Inorg. Chem. 2015, 54, 9656−9663